A microstrip-based Rotman lens for mm-wave sensing operations

Leonard Hall[a], Hedley Hansen[b] and Derek Abbott[a]

[a]Centre for Biomedical Engineering and
Department of Electrical and Electronic Engineering
Adelaide University, SA 5005, Australia
E-mail: lthall@eleceng.adelaide.edu.au

[b]DSTO
EWD, PO Box 1500, Salisbury SA 5108
E-mail: hedley.hansen@dsto.defence.gov.au

ABSTRACT

Rotman lenses offer a compact, rugged and reliable means of forming multi-beam staring array sensing arrangements. The successful implementation of Rotman devices, that operate at mm-wave frequencies, is important to a wide range of applications ranging from covert military operations and collision avoidance in cars and boats in poor weather, to landing aids for aircraft. This paper discusses the development of a Ka-band microstrip-based Rotman lens that is to be used in collision avoidance and other military related roles.

Keywords: Microstrip, Rotman lens, beam-forming, passive detection, radiometry, collision avoidance

1. INTRODUCTION

Sensors operating in the mm-wave (20-100 GHz) band have better poor weather performance than those operating at smaller IR and visible wavelengths. Naturally occurring 37 and 94 GHz radiation propagates through cloud, smoke, fog and other such aerosols, as seen by the attenuation curve in Fig. 1. Millimetre wave systems provide better spatial resolution (and target discrimination) than systems operating at centimetre and metre wavelengths and comprise of very compact, low weight and physically small antennas. These properties make millimetric wave sensors an attractive option in a variety of defence, security-related and civilian remote sensing applications.

Beamforming mm-wave antennas have numerous applications including radar,[1] communication[2,3] and biomedical systems,[4,5] synthetic vision schemes and automobile collision-avoidance systems.[6–13] Collision avoidance Doppler radars operating at 77 GHz are commercially available but of interest here is the development of passive radiometric sensors which promise at least equivalent performance without the disadvantages of active systems. The sensor technique that is to be employed is to be based on biologically inspired insect vision principles[7,14–21] involving motion detection and the system requirements are therefore more relaxed than in full mm-wave imaging systems.

This paper describes the development of a Rotman lens-based antenna array,[22] to be operated at 37 GHz. The design and simulated responses are presented. A characteristic of this design is that it is to be monolithically fabricated so that it provides a low-cost testing platform of the design for further versions at the higher frequencies eg. 94 GHz. These frequencies are chosen because they are centres of atmospheric transmission bands, with the presence of O_2 and H_2O in the atmosphere causing peak absorption of mm-waves at 60 and 22 GHz respectively. The paper also provides an assessment of the expected performance in operation.

2. THE SENSOR WITH SPECIFICATIONS FOR INTEGRATED DESIGN

The radiometric sensor described below employs a beamforming Rotman lens which allows simultaneous scanning or staring array sensing over a large field-of-view. The Rotman lens arrangement consists of a parallel plate region with beam ports and array ports distributed along opposite contours. The central beamport provides equal path lengths to each array element. An offset beam produces a path length and hence a phase gradient along an array giving a steered beam. A Rotman lens approach promises the advantages of inherent wide bandwidth, the possibility of full

Passive Millimeter-Wave Imaging Technology V, Roger M. Smith, Roger Appleby,
Editors, Proceedings of SPIE Vol. 4373 (2001) © 2001 SPIE · 0277-786X/01/$15.00

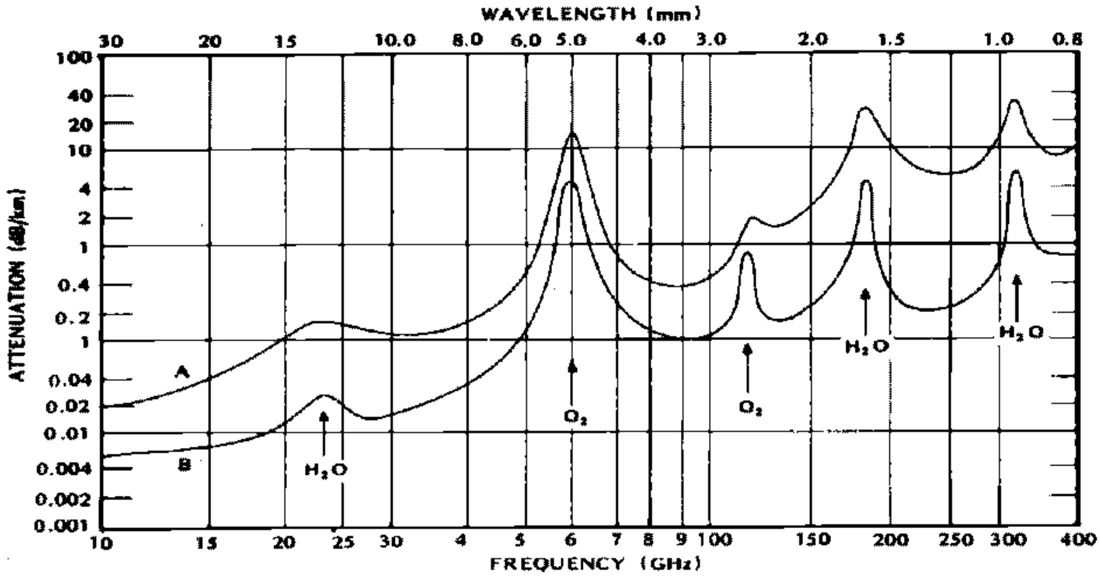

Fig. 1. The one way attenuation of electromagnetic radiation in the troposphere[23]

integration with detection circuitry at mm-wave frequencies and the ability to later employ insect vision detection algorithms through input/output channel discrimination.

The initial design that is being considered is a 35 GHz lens for steering nine beams with a 40° scan angle. This provides a simple prototype to enable rapid development of the skills required for the design's manufacture at affordable cost. In addition in this design, the half-wavelength separation of beamports is achievable and therefore spillover losses can be kept low.

The lens and the feeds are to be implemented using microstrip fed by patch antenna elements. A schematic of the system is shown in Fig. 2(a). This architecture provides a compact structure that is planar and is compatible with monolithic fabrication. It is estimated that a fifteen element array aperture width of 50 mm is achievable at 37 GHz. Apertures of these sizes are suitable for collision-avoidance applications. The theoretical radiation pattern of this system is in Fig. 2(b) showing a scan coverage of 40° for beams of 14° beamwidth and sidelobes levels of -15 dB. The radiation losses through the system arise from dissipation into the substrate through surface wave propagation, interactions at the input microstrip-to-lens transitions, spillover and aberrations within the lens system, interactions at lens-microstrip output feeds and on-chip dissipation. Through appropriate design, the intention is to keep these losses at a minimum.

3. SIMULATION

In order to design the lens a process utilising three levels of simulation is employed. This allows the performance of the device to be adequately predicted before prototype designs are manufactured.

Level one simulation involves the numerical optimisation of the Rotman geometry using ideal models.[24] The lens is modeled using geometric optics. No coupling between input and output ports is considered, with all ports matched and reflections and attenuation ignored.

Level two simulation addresses the non-ideal effects of the microstrip and how adopting various antenna element options affect performance.[25] Level two simulations include optimising the bandwidth performance of the lens.

Level three simulation calculates the impedance at each of the beam ports, array ports and dummy ports, so that effective matching networks can be designed. The various antenna patterns associated with each beam port are therefore provided.

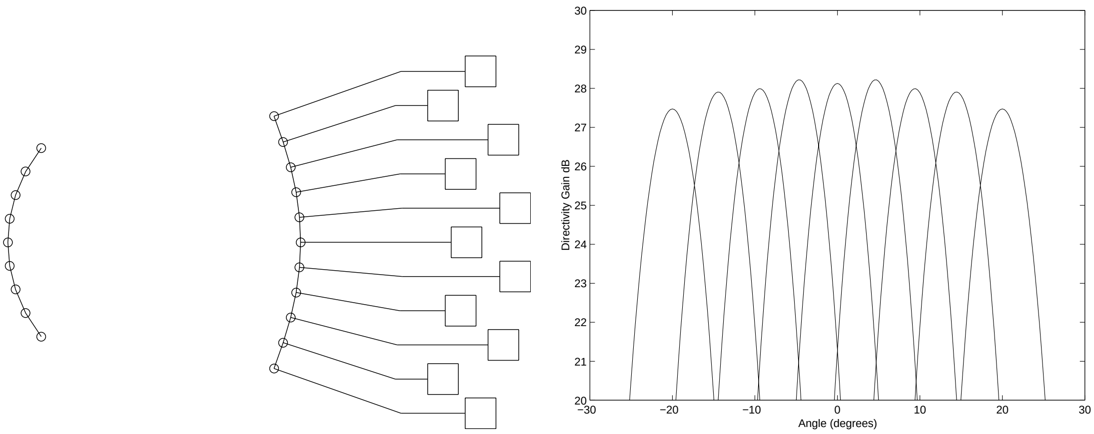

(a) Layout utilising Patch antenna (b) Theoretical radiation pattern

Fig. 2. Basic Rotman Lens Design

3.1. Level 1 and 2, Ideal and Non-Ideal Modeling

Scattering matrices have been used exclusively throughout the simulation. Three scattering matrices have been generated, S_B accounting for the Rotman lens body, S_W for the path delays between antenna elements and associated antenna ports on the inner lens contour and S_A for the phase delays between incoming rays onto the antenna array. Combining these matrices has provided the output at each port due to any given incident wave.

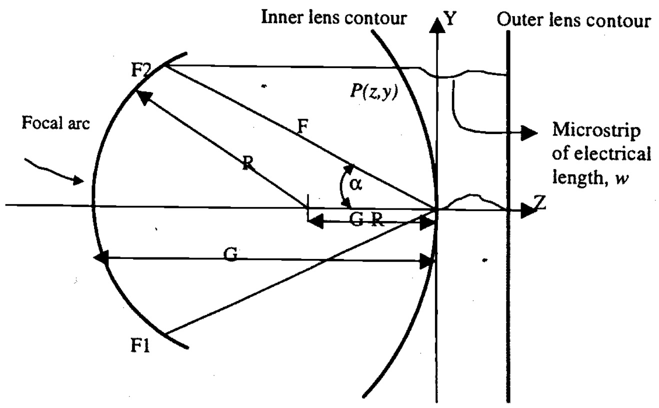

Fig. 3. Rotman Lens Topology[22]

The design of the lens or matrix S_A is governed by the Rotman-Turner design equations. These expressions are given as follows, using the variables defined in Fig.3:

$$
\begin{aligned}
y &= \frac{Y}{F} \\
z &= \frac{Z}{F} \\
n &= \frac{N}{F} \\
g &= \frac{G}{F}
\end{aligned}
$$

$$
\begin{aligned}
w &= \frac{W - W_o}{F} \\
a &= \cos(\alpha) \\
b &= \sin(\alpha) \\
0 &= Aw^2 + Bw + C \\
A &= 1 - \frac{(g-1)^2}{(g-a)^2} - n^2 \\
B &= -2g - n^2 b^2 \frac{g-1}{(g-a)^2} + 2g\frac{g-1}{g-a} \\
C &= -\frac{n^4 b^4}{4(g-a)^2} + g\frac{n^4 b^4}{g-a} - n^2 \\
R &= \frac{(Fa - G)^2 + F^2 b^2}{2(G - Fa)}
\end{aligned}
$$

where $P(Z, Y)$ is the position of the antenna ports, $P(\theta, R)$ is the position of the beam ports N is the position of each antenna in the horizontal plain and W is the added delay length between antenna and lens.

Fig. 2(a) showed the layout of the eleven antenna element, nine beam port configuration under consideration where the opposite contours are clearly shown. The design frequency of the simulations that follow is 37 GHz. A normalised focal length ratio of g = 1.06 is used with the off-axis focal point angle of 20°. Fig. 4(a) shows the desired phase delays between antenna elements and their corresponding antenna ports. Fig. 4(b) displays the maximum phase error versus angle. For the three focal points the phase error is negligible and *between* these points the phase error remains $< 0.7°$. Fig. 5(a) then displays the centre beam of the idealised eleven-beam radiation pattern. The maximum realisable sidelobe level for an array aperture with antenna elements spaced 0.5 wavelengths apart is -30 dB.

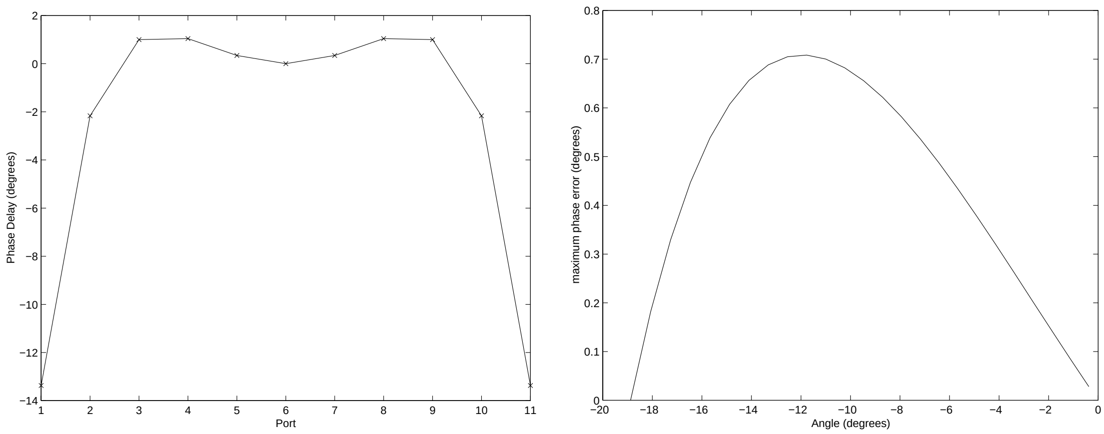

(a) Path delay versus antenna element

(b) Phase error versus beam angle

Fig. 4. Basic Rotman Lens Design

The adverse affect of using non-ideal antenna elements within a microstrip lens structure has been accounted for. Using appropriate S_A and S_W matrices, the losses in the system increase and have a minor effect in shaping the beam radiation patterns.[26] The performance of the lens at frequencies above and below the design frequency has also been considered because as has been shown, this can significantly reduce the efficiency of the system.[26] For the current design, operating at a frequency shifted 10% from the design frequency increases losses by less than 1 dB. This effect is much less than the effect matching networks and patch antenna geometries have on the bandwidth of operation.

3.2. Implementation of Design

Using this model, the effects of various design changes have been examined. Fig. 5(b) shows the design with matching networks between the lens and microstrip lines, and between the lens and the dummy ports. Earlier designs employed a dipole antenna array[13,19,20] due to the possibility of stacking 1-D arrays to form a 2-D coverage. Fig. 5(b) shows patch antenna elements are adopted. Patch antennas have a number of inherent advantages over other antenna designs. They are mounted and matched to the microstrip by a $\lambda/4$ impedance transformer with ease, and they have low levels of cross-coupling. Patch antennas radiate perpendicularly to the surface they are mounted on and this allows them to be moved in the X direction, without disturbing their performance in the Z-Y plane. This feature has been exploited in the design because it allowed greater freedom in accommodating simple microstrip architectures (eg., straight lines) which avoid electromagnetic discontinuities. Moreover, it also allowed an array configuration to be adopted where mutual coupling was reduced to insignificant levels. It should be noted that an important aspect of this patch antenna array structure is the reduction in beam-width in the Z-X plane. This is displayed in Fig. 5(c), where a narrowing of the beam and the lobes on both sides of the main beam is shown.

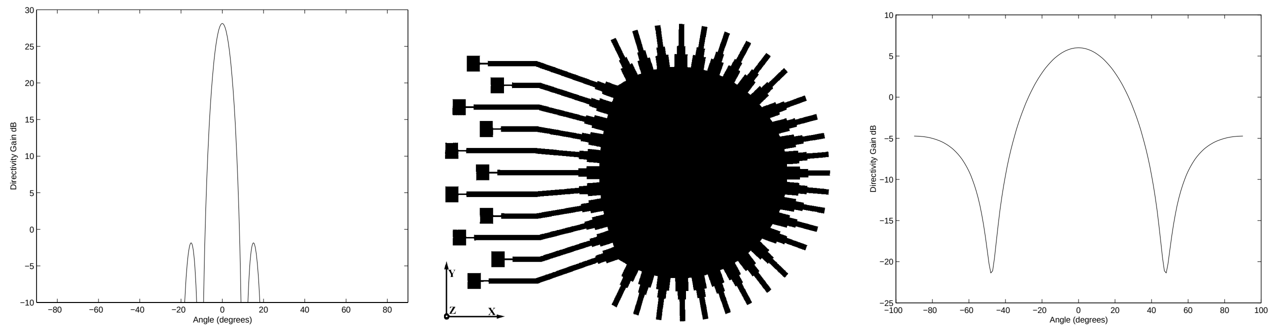

(a) Sidelobe Level

(b) Final Layout

(c) Beam pattern 90° to scan

Fig. 5. Level 2 Simulation Results

To achieve low side lobe levels reflections from the sides of the Rotman lens must be minimised. This has been achieved by matching the ports and filling the gap between the beam and array ports with dummy ports, which are are terminated with a 50 Ω impedance.

3.3. Level 3 - Electromagnetic Modeling

Electromagnetic simulation provides the link between the design, and the final Rotman lens realisation.

This initially involves calculating the impedances of the beam, array, and dummy ports around the body of the lens. Networks then match each of the ports to a 50 Ω line. For narrow bandwidths a quarter wave impedance transformer is adequate, however, for broadband performance, more complicated networks must be used.[27,28] The width of the line connecting the body of the lens to the 50 Ω line, is designed so that only first order modes are allowed to propagate. Higher order modes are then confined to the body of the lens.

The simulated beam pattern associated with the lens comprising matching networks is shown in Fig. 6(a), 6(b) and 6(c). Satisfactory sidelobes of -15 dB between the $\pm 10°$ beam ports, increasing to -10 dB are displayed. The performance of the lens can be further improved by adjusting the angle of the beam ports to optimise the power distribution across the antenna array in order to keep beam squint to a minimum.

The simulations also show that the performance of the antenna array in the Z-X plane agrees closely with the idealised model predictions.

4. COLLISION AVOIDANCE APPLICATION

A radiometer employs front-end circuitry that presents a signal whose voltage level is related to the power of radiation impinging on the radiometer's sensor. There exists two contributions to any measured power, one associated with the antenna signal and another associated with the noise of the measuring system. This has been expressed as

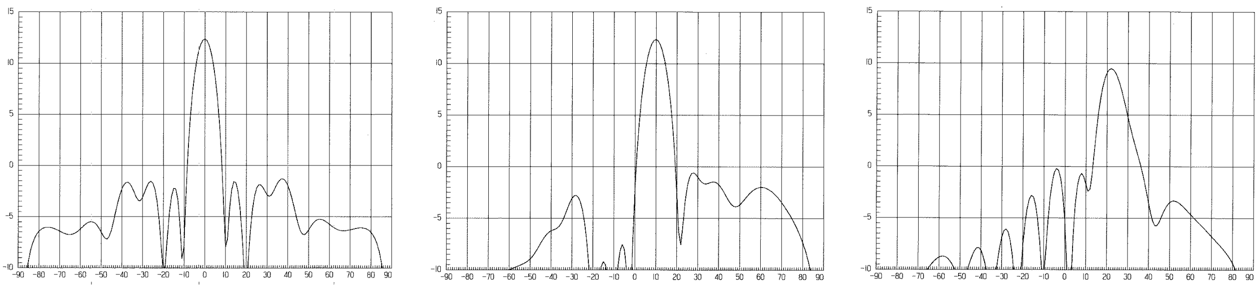

(a) Gain (dB) vs Angle of 0° beam port

(b) Gain (dB) vs Angle of 10° beam port

(c) Gain (dB) vs Angle of 20° beam port

Fig. 6. Results of Electromagnetic simulation

$$P \;=\; kBG(T_A + T_N)$$

where G = gain associated with pre-detector amplification, B = signal bandwidth, k = Boltzmann's constant, T_A = antenna temperature and T_N = temperature of system.

A square-law detector returns a voltage that corresponds to the measured power.

The detection capability of a collision avoidance detector based on the current design has been predicted by evaluating the signal level associated reflective vehicle-sized objects situated at different ranges from the sensor. Fig. 7 depicts the scenario. A different voltage would be recorded when the radiating vehicle is within the sensor's mainbeam compared to when it is not. Most significantly, the relative contributions to the signal level from the object and background radiation depend on the fraction of the mainbeam area covered by the object. The size of the Rotman lens aperture and the operating frequency determine the antenna beamwidth and the mainbeam area increases with the distance R separating the sensor from the object.

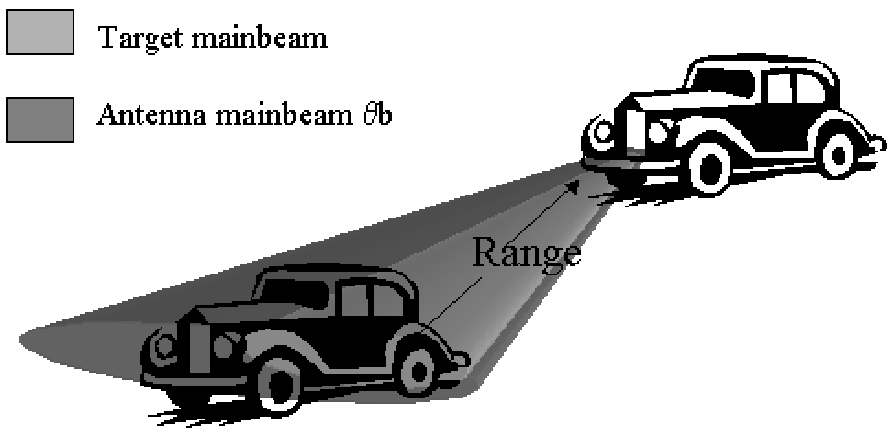

Fig. 7. Depiction of collision avoidance application

Adapting the Wilson et al formalism,[29] Signal to Noise Ratios (SNRs) associated with measuring 35 GHz (wavelength = λ = 8.57 mm) thermal emissions from a car sized object (A = 2 m^2) have been calculated. Fig. 8 shows expected SNR variations with range where the different curves correspond to receivers of differing noise levels being connected to the backend of the designed lens. The parameters used to determine the signal levels are indicated in the figure. The sensor size $D = 42$ mm has been chosen because 11 elements of the Rotman arrangement will cover this distance if spaced $\lambda/2$ apart. The legend outlines noise levels (dB) of detection systems of differing performance levels. The noise T_{noise} in the system depends on the sensitivity of the system expressed as

$$T_{noise} = \frac{T_N}{\sqrt{B.\tau}}$$

where B = bandwidth, and τ = sampling period.

Certainly, radiometer devices with noise levels 15 dB are currently available, and with modern low-noise MMIC's technology , a receiver with the wide-bandwidth low-noise characteristics, needed for the collision avoidance capability shown in curve (i), is achievable.

The horizontal curve in Fig. 8 indicates the SNR considered necessary for object identification[29] (i.e., SNR$\sim$7 dB). Vehicle size objects should be detected at distances ranging from 10 to 40 m, depending on the sensitivity of the detection system.

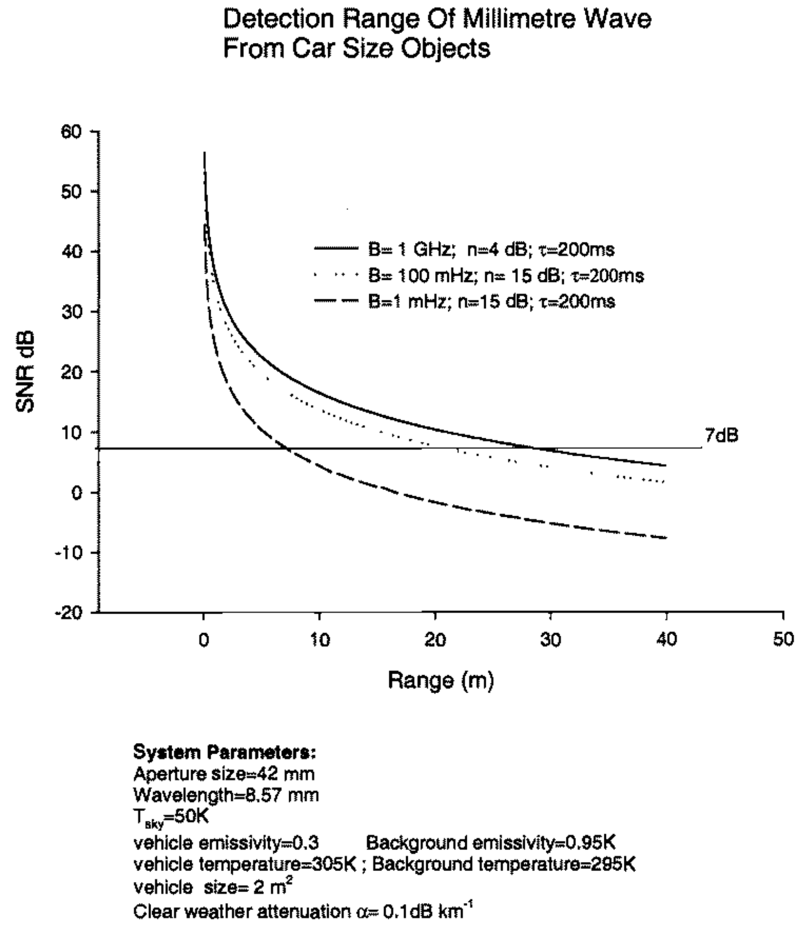

Fig. 8. The predicted operating range of the Rotman lens sensor in collision avoidance applications

5. CONCLUSION

This paper describes the design and simulation of a Ka-band mm-wave sensor for collision avoidance applications. The simulation predicts that the sidelobe levels and mainbeam gain are comparable with similar Rotman lens designs that have been reported elsewhere. If the performance levels predicted by the simulation are achieved on production of the lens, it would form the basis for sensors that are suitable for detecting small vehicles at ranges of <50 metres.

ACKNOWLEDGMENTS

This research is supported by funding from the ARC, the DSTO RF Hub, and the Sir Ross & Sir Keith Smith Fund.

REFERENCES

1. N. C. Currie and C. E. Brown, eds., *Principles and Applications of millimeter-wave radar*, Artech House, 1987.
2. T. Ihara, T. Manabe, M.Fujita, T. Matsui, and Y. Sugimoto, "Research activities on millimeter-wave indoor wireless communication systems at crl," *1995 Fourth IEEE International Conference on Universal Personal Communications* , pp. 197–200, 1995.
3. T. Ihara, Y. Sugimoto, and M. Fjita, "Research and development project for millimeter-wave premises communication systems," *Review of the Communications Research Laboratory* **41**(3), pp. 219–229, 1995.
4. L. O. Boric, Y. Nikawa, W. Snyder, J. Lin, and K. Mizuno, "Novel microwave and millimeter-wave biomedical applications," *4th International Conference on Telecommunications in Modern Satellite, Cable and Broadcasting Services. TELSIKS'99* **1**, pp. 186–193, 1999.
5. O. V. Betskii, N. D. Devyatkov, and V. V. Kislov, "Low intensity millimeter waves in medicine and biology," *Critical Reviews in Biomedical Engineering* **28**(1-2), pp. 247–268, 2000.
6. A. Mohamed, A. Campbell, D. Goodfellow, D. Abbott, H. Hansen, and K. Harvey, "Integrated millimetre wave antenna for early warning detection," in *Proc. SPIE Design, Characterization and Packaging for MEMS and Microelectronics*, pp. 461–469, October 1999.
7. D. Abbott, A. Moini, A. Yakovleff, X. T. Nguyen, A. Blanksby, G. Kim, A. Bouzerdoum, R. E. Bogner, and K. Eshraghian, "A new vlsi smart sensor for collision avoidance inspired by insect vision," *Proc. SPIE Intelligent Vehicle highway Systems* **2344**, pp. 105–115, November 1995.
8. D. Goodfellow, G. P. Harmer, and D. Abbott, "mm-wave collision avoidance sensors: future directions," *Proc. SPIE Sensing and Controls with Intelligent Transportation Systems* **3525**, pp. 352–362, November 1998.
9. D. Abbott, A. Bouzerdoum, and K. Eshraghian, "Two-dimensional smart arrays for collision avoidance," *Proc. SPIE Transportation sensors: Collision Avoidance, Traffic Management and ITS* **3207**, pp. 36–39, October 1998.
10. X. Nguyen, A. Bouzerdoum, R. Bogner, K. Eshraghian, D. Abbott, and A. Moini, "The stair-step tracking algorithm for velocity estimation," *ANZIIS-93* , pp. 412–416, December 1994.
11. A. Yakovleff, D. Abbott, X. T. Nguyen, and K. Eshraghian, "Obstacle avoidance and motion-induced navigation," *CAMP 95 Computer Architectures for Machine Perception Workshop* , pp. 384–393, 1995.
12. K. Chin and D. Abbott, "Motion detection using colour templates," *Proc. SPIE Design, Characterization and Packaging for MEMS and Microelectronics* , pp. 314–323, October 1999.
13. D. C. Goodfellow and D. Abbott, "Collision avoidance for nanosatellite clusters using millimeter-wave radiometric motion sensors," *Proc. SPIE Electronics and Structures for MEMS* **3891**, pp. 276–284, October 1999.
14. D. Abbott, A.Moini, A. Yakovleff, X. Nguyen, R. Beare, W. Kim, A.Bouzerdoum, R. E. Bogner, and K. Eshraghian, "Status of recent developments in collision avoidance using motion detectors based on insect vision," *Proc. SPIE Transportation Sensors and Controls* **2902**, pp. 242–247, November 1997.
15. A. Moini, A. Bouzerdoum, A. Yakovleff, D. Abbott, O. Kim, K. Eshraghian, and R. E. Bogner, "An analog implementation of early visual processing in insects," *International Symposium on VLSI Technology, Systems, and Applications* , pp. 283–287, May 1993.
16. X. T. Nguyen, K. Eshraghian, M. Moini, A. Bouzerdoum, A. Yakofleff, D. Abbott, and R. E. Bogner, "An implementation of smart visual micro-sensor based upon insect vision," *Proc.12 th Aust. Micro. Conf. Microelectronics, Meeting the Needs of Modern Technology* , pp. 129–134, October 1993.
17. A. Moini, A. Bouzerdoum, K. Eshraghian, A. Yakovleff, X. T. Nguyen, A. Blanksby, R. Beare, D. Abbott, , and R. E. Bogner, "An insect vision-based motion detection chip," *IEEE JSSC* **32**, pp. 279–284, Febuary 1997.
18. D. Abbott, A. Yakovleff, A. Moini, X. T. Nguyen, A. Blanksby, R. Beare, A. S. Beaumont, G. Kim, A. Bouzerdoum, R. E. Bogner, and K. Eshraghain, "Biologically inspired obstacle avoidance - a technology independent paradigm," *Proc. SPIE Mobile Robots X* **2591**, pp. 2–12, October 1995.
19. D. Abbott and A. Parfitt, "Collision avoidance device using passive millimetre-wave array based on insect vision," in *Proc. IREE 14th Australian Microelectronics Conference (Micro' 97)*, pp. 201–204, October 1997.
20. D. Abbott and A. J. Parfitt, "Extension of the insect-vision paradigm to millimeter waves," *Proc. SPIE Transportation Sensors* **3207**, pp. 103–106, October 1998.

21. D. Abbott, A. Bouzerdoum, and K. Eshraghian, "Future directions for motion detection based on the parallel computational intelligence of insects," *Proc. 23rd Euromicro Conference New Frontiers of Information Technology Short Contributions* , pp. 244–249, September 1997.
22. W. Rotman and R. F. Turner, "Wide angle microwave lens for line source applications," *IEEE Trans. Antennas Propagate* **AP-11**, pp. 623–632, November 1963.
23. J. Preissner, "The influence of the atmosphere on passive radiometric measurements," *Millimeter and Submillimeter Wave Propagation and Circuits* , pp. 48/1–14, 1979.
24. R. C. Hansen, "Design trades for rotman lenses," *IEEE Trans. Antennas Propagate* **39**, pp. 464–472, April 1991.
25. A. Balanis, *Microwave Engineering*, Harper and Row, 1982.
26. L. Hall, H. Hansen, and D. Abbott, "Design and simulation of a high efficiency rotman lens for mm-wave collision avoidance sensor," *Proc. SPIE Smart Electronics and MEMS* **4304**, December 2000.
27. K. K. Chan, "Planar waveguide model of rotman lens," *1989 IEEE AP-S International Symposium* **2**, pp. 651–654, June 1989.
28. M. Michaelides, "Microstrip transmission lines: impedance matching, coupling and filtering," *Mullard Technical communications* , pp. 170–176, October 1972.
29. W. J. Wilson and et al, "Millimetre wave imiging sensor,," *IEEE trans. Microwave Theory tech.* (MTT-34), pp. 1026–1035, 1986.